Impact of nanometer-scale roughness on contact-angle hysteresis and globulin adsorption

Bert Müller[a)]
Institute of Communication Technology, Computer Vision Laboratory, ETH Zentrum, CH-8092 Zurich, Switzerland

Marco Riedel
ProBioGen, D-13086 Berlin, Germany

Roger Michel, Susan M. De Paul, and Rolf Hofer
Laboratory for Surface Science and Technology, Department of Materials, ETH Zürich, CH-8952 Schlieren, Switzerland

Dietmar Heger and Detlev Grützmacher
Micro- and Nanostructures Laboratory, Paul Scherrer Institute, CH-5232 Villigen-PSI, Switzerland

(Received 13 September 2000; accepted 18 June 2001)

Besides surface chemistry, the surface roughness on the micrometer scale is known to dominate the wetting behavior and the biocompatiblity properties of solid-state materials. The significance of topographic features with nanometer size, however, has yet to be demonstrated. Our approach is based on well-defined Ge nanopyramids naturally grown on Si(001) using ultrahigh vacuum chemical vapor deposition, where the nanopyramid density can be precisely controlled by the growth conditions. Since the geometry of the nanopyramids, often termed dome clusters, is known, the surface roughness can be characterized by the Wenzel ratio with previously unattainable precision. Dynamic contact-angle measurements and adsorption of γ-globulin as a function of that ratio demonstrate the strong correlation between surface nanoarchitecture, on one hand, and wetting behavior and biocompatibility, on the other hand. Related x-ray photoelectron spectroscopy measurements reveal that potential changes of surface composition can be definitely excluded. © *2001 American Vacuum Society.* [DOI: 10.1116/1.1392402]

Biocompatibility is understood as the chemical and structural compatibility of a material integrated in the desired biological environment. Although in the past the focus has often been on the chemical compatibility, recent studies have recognized the importance of surface topography. Curtis and Wilkinson,[1] for example, have pointed out that surface architecture on the micrometer scale tends to have even a greater effect than chemical patterns. The significance of topographic features with micrometer size has also been clearly demonstrated in other studies.[2–8] The significance of features on the nanometer scale in phenomena such as wetting and protein adsorption, however, is still unclear.[9–12] One problem is related to the quantification of surface roughness. Therefore, it is highly desirable to fabricate well-defined nanostructured surfaces, which can serve as ideal substrates for fundamental experiments in the field of biomaterials science. Such nanostructures can be formed by germanium islands grown on Si(001). The island density, shape, and size distribution can be tailored by adjusting the growth conditions.[13]

The preparation of silicon surfaces with atomically flat terraces of micrometer size is known.[14–18] Germanium, which has a 4% larger lattice constant than silicon, grows on Si(001) by the layer plus island mode (Stranski–Krastanov growth mode). The Ge wetting layer, a uniformly strained film, grows pseudomorphically up to a thickness of 2–3 monolayers, followed by the formation of three-dimensional Ge islands on top of the uniform film.[16,19] These islands have a pyramidal or prism-like shape and are free of dislocations.[19] At lower coverages the nanopyramids are square or elongated huts with {105} facets, forming angles of 11.3° with the flat substrate.[16] These hut clusters with a base of 60 nm×60 nm are about 6 nm high. Their formation can be followed using high temperature scanning tunneling microscopy (STM).[20]

At higher coverages the shape changes, and nanopyramids, termed dome clusters, form.[21–23] Here, the side planes are {113} and {102} facets, which give rise to angles of 25.2° and 26.6°, respectively. Their bases are comparable with those of hut clusters, but their heights are greater by more than a factor of 2. The observed shape changes are attributed to transitions in the growth of strained islands.[24–26] Since the strain determines the island shape, one can take advantage of submonolayer carbon predeposition to produce smaller pyramids with a top facet.[27,28] This means that by adjusting the island volume and the strain energy at the Ge–Si interface, one finds six distinct island shapes including top, shallow, and steep facets.[25] The size of the islands can be significantly increased by annealing, whereby the island shape can change from islands with steeper facets (domes) back to huts.[29–32] In addition, the island size distribution can be tailored by self-organization during the growth of multilayer Ge/Si sandwich

[a)]Author to whom correspondence should be addressed; electronic mail: bmueller@vision.ee.ethz.ch

structures.[33–36] The multilayer arrays of coherently strained islands result in progressively more uniform island sizes and spacings irrespective of their initial density.

It should be mentioned that the formation of these islands on the wetting layer proceeds via a precursor array of shallow, stepped mounds on the surface that result from the strain-driven growth instability.[37,38]

Although most of the reported studies of growth of germanium islands on Si(001) are based on molecular beam epitaxy because surface sensitive methods such as electron diffraction can be applied, a limited number of publications related to chemical vapor deposition has been reported.[39–41] The islands found at a coverage of about 12 monolayers have a narrow island height distribution of (15 ± 1) nm and a diameter of about 70 nm.[41] For the present study, such islands have also been prepared by ultrahigh vacuum chemical vapor deposition. Related *ex situ* atomic force microscopy (AFM) images are represented in Fig. 1. These images qualitatively show the increase in surface roughness with increasing nanopyramid density.

After the silicon substrate with the germanium nanopyramids was exposed to air, the sample was oxidized. The x-ray photoelectron spectroscopy (XPS) data of Fig. 2 reveal that the Ge wetting layer is fully oxidized, whereas the nanopyramids are only covered by a thin oxide film. The thin oxide film on the pyramids, however, does not significantly modify the pyramid geometry. The statement is corroborated by the AFM height measurements, which lead to an almost constant mean nanopyramid height of (15 ± 3) nm in agreement with *in situ* STM measurements. Certainly, possible subtle effects associated with the strain of the native oxide may deform the pyramids or change their facet structure. The strain may expand the island surface, inducing depressions around the islands.[41] These effects, however, seem to be of minor importance.

The AFM images directly provide the surface morphology. However, quantification of the surface roughness using the AFM images with different island densities is generally unreliable. As shown in Table I, the data for the root-mean-square (rms) roughness and average roughness as well as the extracted effective surface depend significantly on the scanning range, the surface features, and their distribution. Consequently, these data cannot be used for the quantitative analysis of nanometer-scale surface roughness.

A promising alternative, demonstrated here, is island counting over a certain area for the different samples to determine the island density. Since the height of the nanopyramids can be precisely measured by the AFM and the shape of the dome pyramids is known, the effective surface comes to light. The roughness factor (Wenzel ratio) is defined by the ratio of the effective surface to the projected one. For pyramids, the fraction of the surface that is covered by the islands has to be weighted by the inverse cosine of the facet angle. Hence, even a potential shape change of the nanopyramids due to the native oxide can be parameterized simply by an additional factor.

It has been reported that surface roughness modifies the

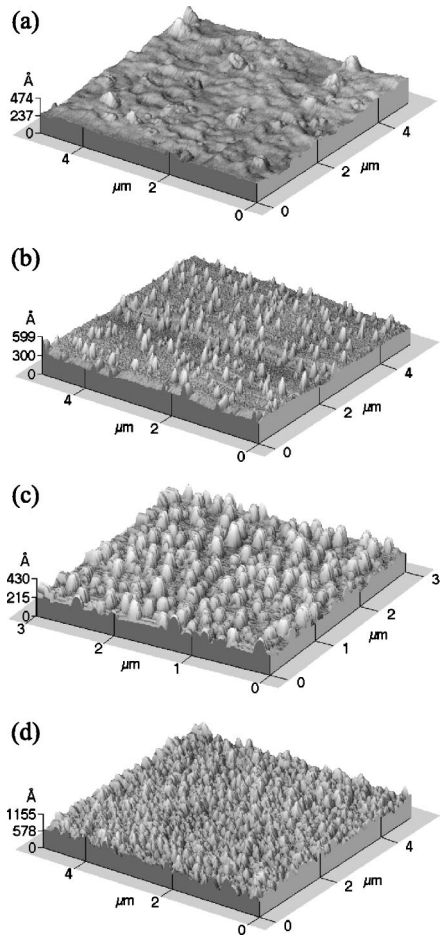

FIG. 1. AFM images characterizing the surface roughness and nanopyramid density. The images are obtained by the use of AUTOPROBE CP (Park Scientific Instruments, California). The nanopyramidal surfaces were prepared on 4 in. Si(001) wafers purchased from Sico Meiningen Wafer GmbH, Germany, by ultrahigh vacuum chemical vapor deposition under the following conditions: (a) flow of 4×20 mL/3 mL silane/germane followed by 20 mL silane capping at a substrate temperature of 600 °C and a total pressure of 3.3×10^{-4} mbar, (b) mixture of 20 mL silane with 0, 3, 7, 13, 20, 30 mL germane followed by 20 mL silane and 20 mL germane at a substrate temperature of 550 °C and a total pressure of 1.3×10^{-4} mbar, (c) consecutive flow of 60 mL silane, mixture of 20 mL silane with 40 mL germane, 40 mL silane, and 20 mL germane at a substrate temperature of 520 °C and a total pressure of 6.7×10^{-5} mbar, (d) 20 mL silane with 0, 3, 8, 15, 22, 0, 30, 0 mL germane followed by 20 mL germane at a substrate temperature of 600 °C and a total pressure of 1.5×10^{-4} mbar.

contact angles and the contact-angle hysteresis of wetting. In general, it is claimed that the contact angles are greater on rough surfaces than on smooth surfaces and that the wetting hysteresis increases with the surface roughness.[42] However, sometimes the same authors state that surface roughness has no definite effect on the contact angle.[43] For contact angles smaller than 90°, the contact angle can even decrease with surface roughness, which can be explained by the capillary effect.[44]

Such inconsistencies can often be related to the qualitative characterization of the surface roughness, e.g., ''highly polished,'' or to the ambiguous rms roughness determination by the scanning probe techniques as discussed earlier. Furthermore, very recently wetting and dewetting studies on sur-

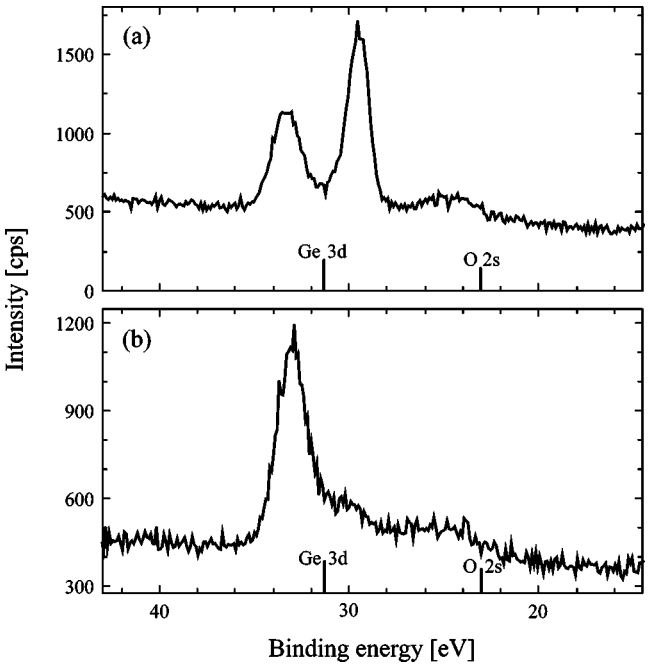

FIG. 2. XPS Ge_{3d} high-resolution spectra of (a) Ge nanopyramids, CVD grown at 600 °C with Si capping [cf. Fig. 1(a)] and (b) 2.4 monolayer Ge wetting layer on Si(001) grown by molecular beam epitaxy. Two different binding energies of germanium were detected and attributed to elemental Ge (29.5 eV) and GeO_2 (33.3 eV), indicating a fully oxidized Ge wetting layer. The ratio of GeO_2 to Ge for the nanopyramidial surfaces suggests that this layer thickness is in the range of a few monolayers with no significant differences in binding energy among the samples investigated.

faces that were structured on the micrometer scale have uncovered shape changes of the droplet associated with morphological transitions.[45–47] Hence, the well-accepted Young's equation is not satisfied for small enough domains.

Therefore, the question arises how far nanometer-scale surface morphology controls the contact angle and its hysteresis. The answer is important for very different applications including pharmaceutical,[48] tribological, and conduction phenomena.[49] Presumably, it also plays a significant role in biocompatibility.[50–52]

Since Young established the relation between the interfacial energies and the contact angle, wetting has been understood as a thermodynamic phenomenon.[53] Therefore, Wenzel introduced the roughness factor, the ratio of the effective to the projected surface, to parameterize the surface roughness.[54] He justified the roughness factor by the statement that within a measured unit area of a rough surface the intensity of the surface energy is greater than in the corresponding area on a smooth surface. Although various experimental studies have depicted this effect qualitatively, the Wenzel ratio was not detected exactly.[44] Since the Wenzel ratio can be exactly determined for pyramidal surfaces, it is worth correlating the contact angle with the roughness factor. Silicon and germanium substrates covered by their native oxides are known to be very hydrophilic. Typical contact angle values for water are around 40°.[55–58] This angle is already rather small, and measurements of contact angles below 15° exhibit large error bars. Water, the liquid with the highest possible liquid-vapor interfacial energy and, therefore, the highest possible contact angle,[59] is also used in the present study. The problem here is the fact that the result strongly depends on the ambient conditions, namely the humidity. Therefore, direct measurements of the equilibrium Young's angle as a function of nanometer-scale roughness are crude. An experiment that is much more reproducible is the dynamic measurement of the advancing and the receding contact angles. Again, the results depend crucially on the ambient conditions. Therefore, it was decided to measure the dynamic contact angles on the different substrates immediately after prewashing the surface. An atomically thin water film covers the surface but does not equalize the roughness. Consequently, the measurement becomes reproducible.

The results show that the advancing contact angle of water monotonically increase by 20° from the flat substrates [cf.

TABLE I. Characterization of surface roughness; AFM scan size in brackets. rms and average roughness are determined by the computer code ProScan Image Processing version 1.5.1 of Park Scientific Instruments. The relative effective surface that should correspond to the roughness factor is calculated from AFM images with a size of 5 μm×5 μm by use of the computer code IMAGE SXM V1.62. The pyramid density is derived from a series of AFM images with scanning ranges between 1 and 10 μm. Deviations from image to image are typically well below 10%.

Substrate	rms roughness (nm)	Average roughness (nm)	Relative effective surface	Pyramid density (10^{-12} m^{-2})	Roughness factor r
a	3.7 (5 μm)	2.7 (5 μm)	1.001 (5 μm)	0.84	1.001
	5.1 (10 μm)	3.2 (10 μm)	1.001 (10 μm)		
b	4.7 (2.5 μm)	3.1 (2.5 μm)	1.010 (2.5 μm)	12.56	1.021
	5.1 (5 μm)	3.6 (5 μm)	1.006 (5 μm)		
	7.5 (10 μm)	6.0 (10 μm)	1.004 (10 μm)		
c	5.7 (2.5 μm)	4.5 (2.5 μm)	1.018 (2.5 μm)	26.08	1.044
	5.8 (5 μm)	4.6 (5 μm)	1.012 (5 μm)		
	6.1 (10 μm)	4.6 (10 μm)	1.008 (10 μm)		
d	11.4 (2.5 μm)	9.0 (2.5 μm)	1.072 (2.5 μm)	40.16	1.068
	12.0 (5 μm)	9.0 (5 μm)	1.048 (5 μm)		
	13.0 (10 μm)	10.0 (10 μm)	1.027 (10 μm)		

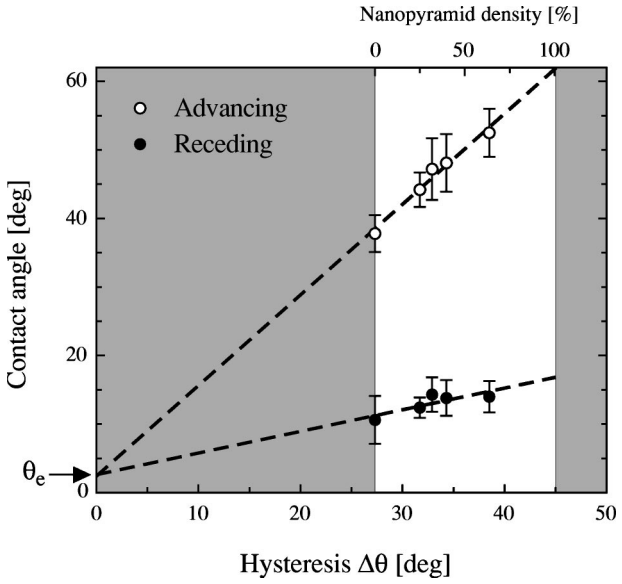

FIG. 3. Advancing (open circles) and receding (filled circles) contact angles vs contact angle hysteresis for water on surfaces with different nanopyramid density. The dashed lines correspond to the linear regressions. The gray-colored regions are not accessible by the measurement. The Young's angle, θ_e, derived is close to zero. Note that the presentation does not directly contain the surface roughness. The contact angles were determined by increasing and decreasing the size of an ultrapure water droplet in ten steps with the G2 system (Kruess, Germany). The experiment was repeated six times to obtain reasonable statistics.

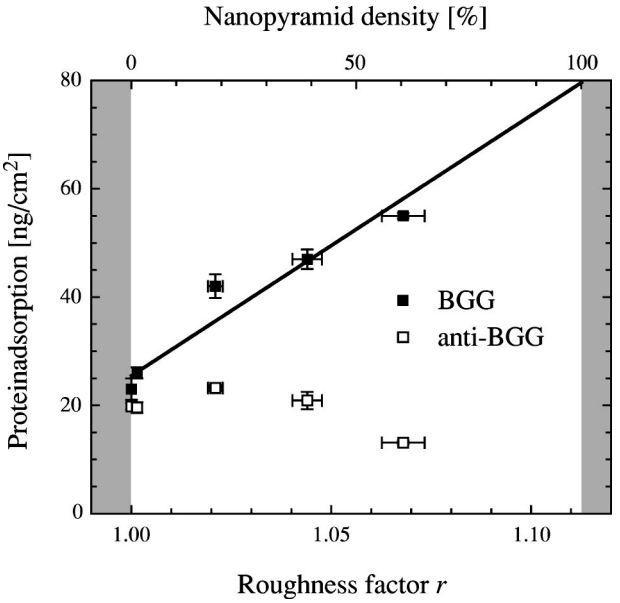

FIG. 4. Protein adsorption of BGG and anti-BGG vs roughness factor. Although the effective surface only increases by 7%, the amount of adsorbed BGG is more than a factor of 2 higher on the rough than on the flat substrate, demonstrating the existence of preferred nucleation sites at the nanopyramids.

Fig. 1(a)] to substrates with maximum pyramid density [Fig. 1(d)], whereby the receding contact angle remains constant within the error bars. Note that the contact angle measurement is rather difficult for values below 15°. This means that the contact-angle hysteresis, which is the difference between the advancing and the receding angles, increases with the surface roughness. From the intersection of the fits for advancing and receding angles versus contact angle hysteresis, $\Delta\theta$, with the ordinate at $\Delta\theta=0$, one finds the equilibrium contact angle θ_e[44] (cf. Fig. 3). We attribute the result that the equilibrium angle is close to zero to the water pretreatment. This result also explains our failure to determine the contact angle of an air bubble below these substrates when they were immersed in water (captive bubble method). It was impossible to bring the bubble into contact with the substrate, it always moved away.

The current understanding of contact-angle hysteresis, however, has a preliminary character. Although wetting hysteresis has been theoretically treated on idealized surfaces with nanometer-scale roughness[60] and even on a molecular scale,[61] the phenomenon is not fully understood. First, the influence of drop size[62] and spreading velocity has to be clarified by experiments. Second, although the contact-angle hysteresis can be partly explained by the barrier effect, which gives rise to a symmetric hysteresis,[44] and the capillary effect, which leads to a contact angle reduction,[44,53,63] another phenomenon must also exist to describe the hysteresis shown in Fig. 3.

The biocompatible properties of a material (substrate) are closely related to the adsorption of different proteins. Many authors have treated this issue, e.g., Andrade[64–66] Lundström,[67–69] Norde,[70,71] and Brash.[72,73] The current understanding of protein adsorption includes not only effects such as binding and interfacial thermodynamics but also conformational changes, which can induce tremendous alterations in the biocompatible properties of implant materials. These alterations can be important for γ-globulin, often also termed immunoglobulin *G*, since these proteins are responsible for the humoral immune response. Therefore, we have selected bovine γ-globulin (BGG) for the present study along with bovine serum albumin (BSA), the protein with the highest concentration in serum. Both proteins have sizes comparable to the nanopyramids. Consequently, one may assume that the presence of nanopyramids modifies the protein adsorption and activity.

Indeed, the amount of the adsorbed proteins BSA and BGG, labeled with fluorescein isothiocyanate, significantly increases with the density of nanopyramids on the substrate.[74] The data quantitatively obtained by fluorescence spectroscopy for BGG are shown in Fig. 4. On the flat germanium substrate without pyramids about 20 ng/cm^2 of BGG adsorb. Increasing the effective surface by 7% causes the amount of adsorbed protein to rise by a factor of 2 or 3. This means that the adsorption sites are different on the flat and the pyramidal surfaces. The nanopyramids provide effective adsorption sites for BGG.

The strong protein-substrate binding at the nanopyramids can modify the conformation of the proteins and thereby their activity.[75,76] Here, protein activity is understood as the capability of molecular recognition such as the affinity interactions between BGG and anti-BGG-peroxidase. Using fluorescence measurements we have found that the amount of

TABLE II. XPS-determined atomic percentages for two series of the chemical vapor deposition (CVD)-grown samples and two reference samples [2.4 monolayer Ge film on Si(001) and the bare silicon]. Since the samples were grown under different conditions (cf. figure caption of Fig. 1), the concentrations of silicon and germanium have been added to facilitate comparison. Within experimental error, there is no correlation between surface roughness and surface composition.

Substrate	Roughness factor	Series No.	C(%)	O(%)	Si(%)+Ge(%)
a	1.001	1	7.7	42.2	36.5+13.6=50.1
		2	8.7	41.3	34.8+15.2=50.0
b	1.021	1	8.5	46.9	26.3+18.3=44.6
		2	15.2	41.0	27.5+16.3=43.8
c	1.044	1	8.1	46.2	26.8+19.0=45.8
		2	8.9	47.4	27.2+16.5=43.7
d	1.068	1	9.3	45.4	32.8+12.4=45.2
		2	13.0	42.2	32.1+12.8=44.9
Ge/Si	1.000	1	11.7	39.4	40.1+8.8=48.9
		2	11.7	42.7	40.0+5.6=45.6
Si	1.000	1	14.2	31.8	54.1+0=54.1

biologically active BGG does not scale with the adsorbed BGG. It is even lowered on the substrate with a high nanopyramid density (cf. Fig. 4). On the flat substrates without pyramids, BGG is almost completely active. The relative activity of BGG decreases with pyramid density. This observation implies that on the substrate fully covered by nanopyramids BGG is totally inactive. The linear fit shows that BGG already becomes inactive well below the maximal nanopyramid density associated with the domination of the nanopyramid ledges in BGG adsorption. Consequently, the adsorption sites on the nanopyramids change the conformation of the protein. These results are supported by a related study of monocyte activation on the Ge nanopyramids.[74] Monocytes and especially the monocyte-like cells of the cell line U 937 contain a special receptor, $F_c\gamma IIR$. This receptor allows interactions with the intact F_c (fragment crystallizable) fragments of BGG as present in bovine serum. This kind of interaction leads to the activation of the monocytes, which is characterized by the self-amplified expression of the cytokines interleukin-1β (IL-1β) and tumor necrosis factor (TNF-α).[77,78]

These results give rise to speculations that nanopyramid density not only changes the surface morphology but also the surface chemistry. In order to confirm our hypothesis that the surface chemistry is of minor importance, we have performed XPS experiments on the bare substrates with different pyramid densities. The spectra were recorded on a SAGE 100 (SPECS, Berlin, Germany) using nonmonochromatized Mg $K\alpha$ radiation with an energy of 240 W (12 kV, 20 mA), an electron takeoff angle of 90°, and an electron detector pass energy of 50 eV for survey and 14 eV for detail spectra. For the high-resolution spectra, the Ag $3d_{5/2}$ full width at half maximum corresponds to 1.0 eV. During analysis, the base pressure remained below 1×10^{-8} Pa. All peaks were referenced to the C_{1s} (hydrocarbon contamination) contribution at 285.0 eV.[79]

The survey spectra of the samples reveal the presence of carbon in addition to the expected germanium, silicon, and oxygen peaks. No further elements were detected. High-resolution XPS spectra were, therefore, acquired for C_{1s}, O_{1s}, Si_{2s}, and Ge_{3d} (Table II). The amount of carbon C_{1s} due to adsorbed hydrocarbons is low (usually $\leqslant$10 at. %). It is the result of adventitious hydrocarbon contamination upon removal of the sample from the vacuum chamber and exposure to air, which is commonly observed for metal oxide surfaces.[80] The metallic character of silicon and germanium surfaces is verified by the high-resolution STM images.

The variation in the chemical composition of the two independent sample series was within the error bar of our XPS setup. We were unable to detect any correlation between surface roughness and chemical composition including the adsorbed hydrocarbons. Although changes in surface roughness can influence the ratio of the XPS signal from substrate and overlayer this ratio is almost unaffected for nanometer-scale roughness, especially for the rather flat nanopyramids. Therefore, we conclude that the observed wetting and protein adsorption behavior is primarily due to the nanopyramidal surface morphology.

In conclusion, epitaxial growth of germanium on Si(001) can be used to realize different densities of nanopyramids of identical shape without the use of any lithographic technique. By counting the nanopyramids, the effective surface and, thus, the roughness factor (Wenzel's ratio) can be determined with high precision. Since the study is focused on dome clusters with facets, which form an angle of about 26° with the substrate, the roughness factor can be varied between 1.0000 and 1.1126. The nanopyramids give rise to a strong interaction of BGG with the substrate, changing the protein conformation. The BGG adsorbed on the nanopyramids is inactive. Since we were unable to detect any relation between surface chemistry and wetting behavior/protein adsorption for the nanopyramidal substrates investigated, we conclude that structural elements on the nanometer scale such as nanopyramids can drastically change surface properties including biocompatibility. The tailoring of nanostructures on implant surfaces could improve their properties with respect to function and long-term stability.

The authors thank Marcus Textor (ETH Zürich) for his support of the contact-angle and XPS measurements and Erich Wintermantel (TU München) for his valuable help in initiating this project.

Presented at the 47th International AVS Symposium, Boston, MA, 2–6 October 2000.

[1]A. Curtis and C. Wilkinson, Biochem. Soc. Symp. **65**, 15 (1999).
[2]D. M. Brunette, Int. J. Oral Maxillofac. Implants **3**, 231 (1988).
[3]B. Chehroudi, T. R. Gould, and D. M. Brunette, J. Biomed. Mater. Res. **25**, 387 (1991).
[4]C. Larsson *et al.*, Biomaterials **15**, 1062 (1994).
[5]R. Singhvi *et al.*, Science **264**, 696 (1994).
[6]L. Chou *et al.*, J. Cell. Sci. **108**, 1563 (1995).
[7]E. T. den Braber *et al.*, Biomaterials **17**, 1093 (1996).
[8]B. Chehroudi, D. McDonnell, and D. M. Brunette, J. Biomed. Mater. Res. **34**, 279 (1997).
[9]H. Suzuki *et al.*, Jpn. J. Appl. Phys., Part 1 **34**, 3937 (1995).
[10]T. J. Webster, R. W. Siegel, and R. Bizios, Biomaterials **20**, 1221 (1999).
[11]J. R. Dennis, J. Howard, and V. Vogel, Nanotechnology **10**, 232 (1999).
[12]L. Smith *et al.* (unpublished).
[13]B. Müller, Surf. Rev. Lett. **8**, 169 (2001).
[14]J. M. Marèe *et al.*, Surf. Sci. **191**, 305 (1987).
[15]Y.-W. Mo *et al.*, J. Vac. Sci. Technol. B **8**, 232 (1990).
[16]Y. W. Mo *et al.*, Phys. Rev. Lett. **65**, 1020 (1990).
[17]Y. W. Mo *et al.*, Phys. Rev. Lett. **66**, 1998 (1991).
[18]U. Köhler *et al.*, Ultramicroscopy **42–44**, 832 (1992).
[19]D. J. Eaglesham and M. Cerullo, Phys. Rev. Lett. **64**, 1943 (1990).
[20]M. Kästner and B. Voigtländer, Phys. Rev. Lett. **82**, 2745 (1999).
[21]F. M. Ross, J. Tersoff, and R. M. Tromp, Phys. Rev. Lett. **80**, 984 (1998).
[22]G. Medeiros-Ribeiro *et al.*, Science **279**, 353 (1998).
[23]F. M. Ross, R. M. Tromp, and M. C. Reuter, Science **286**, 1931 (1999).
[24]O. V. Kolosov *et al.*, Phys. Rev. Lett. **81**, 1046 (1998).
[25]I. Daruka, J. Tersoff, and A.-L. Barabasi, Phys. Rev. Lett. **82**, 2753 (1999).
[26]L. G. Wang *et al.*, Phys. Rev. Lett. **82**, 4042 (1999).
[27]O. Leifeld *et al.*, Mater. Res. Soc. Symp. Proc. **533**, 183 (1998).
[28]O. Leifeld *et al.*, Appl. Phys. Lett. **74**, 994 (1999).
[29]T. I. Kamins and R. S. Williams, Surf. Sci. **405**, L580 (1998).
[30]G. Medeiros-Ribeiro *et al.*, Phys. Rev. B **58**, 3533 (1998).
[31]T. I. Kamins *et al.*, Appl. Phys. A: Mater. Sci. Process. **67**, 727 (1998).
[32]T. I. Kamins *et al.*, J. Appl. Phys. **85**, 1159 (1999).
[33]J. Tersoff, Phys. Rev. Lett. **76**, 1675 (1996).
[34]C. Teichert *et al.*, Phys. Rev. B **53**, 16334 (1996).
[35]C. Teichert, J. C. Bean, and M. G. Lagally, Appl. Phys. A: Mater. Sci. Process. **67**, 675 (1998).
[36]F. Liu *et al.*, Phys. Rev. Lett. **82**, 2528 (1999).
[37]P. Sutter and M. G. Lagally, Phys. Rev. Lett. **84**, 4637 (2000).
[38]R. M. Tromp, F. M. Roos, and M. C. Reuter, Phys. Rev. Lett. **84**, 4641 (2000).
[39]B. Cunningham, J. O. Chu, and S. Akbar, Appl. Phys. Lett. **59**, 3574 (1991).
[40]A. Hartmann *et al.*, Meas. Sci. Technol. **11**, 410 (1995).
[41]T. I. Kamins *et al.*, J. Appl. Phys. **81**, 211 (1997).
[42]R. H. Dettre and R. E. Johnson, Jr., Adv. Chem. Ser. **43**, 136 (1964).
[43]J. J. Bikerman, J. Phys. Colloid Chem. **54**, 653 (1950).
[44]H. Kamusewitz, W. Possart, and D. Paul, Colloids Surf., A **156**, 271 (1999).
[45]P. Lenz and R. Lipowsky, Phys. Rev. Lett. **80**, 1920 (1998).
[46]H. Gau *et al.*, Science **283**, 46 (1999).
[47]R. Lipowsky, P. Lenz, and P. S. Swan, Colloids Surf., A **161**, 3 (2000).
[48]G. Zografi and B. A. Johnson, Int. J. Pharm. **22**, 159 (1984).
[49]K. L. Woo and T. R. Thomas, Wear **58**, 331 (1980).
[50]J. Vienken *et al.*, Artif. Organs **19**, 398 (1995).
[51]J. H. Lee *et al.*, Biomaterials **18**, 351–358 (1997).
[52]T. Knoell *et al.*, J. Membr. Sci. **157**, 117 (1999).
[53]L. W. Schwartz and S. Garoff, Langmuir **1**, 219 (1985).
[54]R. N. Wenzel, Ind. Eng. Chem. **28**, 988 (1936).
[55]K. A. Vetelino *et al.*, Int. J. Microcircuits Electron. Packag. **19**, 212 (1996).
[56]E. Fadda *et al.*, J. Adhes. Sci. Technol. **10**, 1067 (1996).
[57]I.-M. Lee and C. G. Takoudis, J. Vac. Sci. Technol. A **15**, 3154 (1997).
[58]L. D. Eske and D. W. Galipeau, Colloids Surf., A **154**, 33 (1999).
[59]D. Y. Kwok and A. W. Neumann, Colloids Surf., A **161**, 31 (2000).
[60]R. E. Johnson, Jr. and R. H. Dettre, Adv. Chem. Ser. **43**, 112 (1964).
[61]W. Jin and J. Koplik, Phys. Rev. Lett. **78**, 1520 (1997).
[62]W. J. Herzberg and J. E. Marian, J. Colloid Interface Sci. **33**, 161 (1970).
[63]L. W. Schwartz and S. Garoff, J. Colloid Interface Sci. **106**, 422 (1985).
[64]D. E. Dong, J. D. Andrade, and D. L. Coleman, J. Biomed. Mater. Res. **21**, 683 (1987).
[65]L. Feng and J. D. Andrade, Biomaterials **15**, 323 (1994).
[66]L. Feng and J. D. Andrade, J. Biomed. Mater. Res. **28**, 735 (1994).
[67]B. Walivaara *et al.*, J. Biomed. Mater. Res. **26**, 1205 (1992).
[68]P. Tengvall, A. Askendal, and I. Lundström, Biomaterials **19**, 935 (1998).
[69]P. Tengvall, I. Lundström, and B. Liedberg, Biomaterials **19**, 407 (1998).
[70]J. G. Fraaije, W. Norde, and J. Lyklema, Biophys. Chem. **41**, 263 (1991).
[71]K. Kawasaki *et al.*, Caries Res. **33**, 473 (1999).
[72]J. L. Brash and P. Ten-Hove, J. Biomater. Sci., Polym. Ed. **4**, 591 (1993).
[73]T. A. Horbett and J. L. Brash, *207th National Meeting of the American Chemical Society, San Diego, CA, 13–17 March 1994* (American Chemical Society, Washington, DC, 1995).
[74]M. Riedel, B. Müller, and E. Wintermantel, Biomaterials **22**, 2307 (2001).
[75]M. Wahlgren and T. Arnebrant, Trends Biotechnol. **9**, 201 (1991).
[76]P. A. Underwood, J. G. Steele, and B. A. Dalton, J. Cell. Sci. **104**, 793 (1993).
[77]C. A. Dinarello, in *Interleukin-1, Inflammation and Disease*, edited by R. Bomford and B. Henderson (Elsevier, Amsterdam, 1989), pp. 17–28.
[78]A. Gearing and R. Thorpe, in *Interleukin-1, Inflammation and Disease*, edited by R. Bomford and B. Henderson (Elsevier, Amsterdam, 1989), pp. 79–91.
[79]C. D. Wagner *et al.*, *Handbook of X-Ray Photoelectron Spectroscopy* (Perkin Elmer, Eden Prairie, MN, 1979).
[80]D. R. Cousens *et al.*, Surf. Interface Anal. **29**, 23 (2000).